BIOCHEMISTRY
including biophysical chemistry & molecular biology

Article

pubs.acs.org/biochemistry

Implications of Binding Mode and Active Site Flexibility for Inhibitor Potency against the Salicylate Synthase from *Mycobacterium tuberculosis*

Gamma Chi,[†] Alexandra Manos-Turvey,[‡] Patrick D. O'Connor,[§] Jodie M. Johnston,[†] Genevieve L. Evans,[†] Edward N. Baker,[†] Richard J. Payne,[‡] J. Shaun Lott,*[,†] and Esther M. M. Bulloch*[,†]

[†]School of Biological Sciences and Maurice Wilkins Centre for Molecular Biodiscovery, The University of Auckland, 3 Symonds Street, Private Bag 92019, Auckland 1142, New Zealand

[‡]School of Chemistry, The University of Sydney, Sydney, NSW 2006, Australia

[§]Auckland Cancer Society Research Centre, Faculty of Medical and Health Sciences, The University of Auckland, Private Bag 92019, Auckland, New Zealand

Supporting Information

ABSTRACT: MbtI is the salicylate synthase that catalyzes the first committed step in the synthesis of the iron chelating compound mycobactin in *Mycobacterium tuberculosis*. We previously developed a series of aromatic inhibitors against MbtI based on the reaction intermediate for this enzyme, isochorismate. The most potent of these inhibitors had hydrophobic substituents, ranging in size from a methyl to a phenyl group, appended to the terminal alkene of the enolpyruvyl group. These compounds exhibited low micromolar inhibition constants against MbtI and were at least an order of magnitude more potent than the parental compound for the series, which carries a native enolpyruvyl group. In this study, we sought to understand how the substituted enolpyruvyl group confers greater potency, by determining cocrystal structures of MbtI with six inhibitors from the series. A switch in binding mode at the MbtI active site is observed for inhibitors carrying a substituted enolpyruvyl group, relative to the parental compound. Computational studies suggest that the change in binding mode, and higher potency, is due to the effect of the substituents on the conformational landscape of the core inhibitor structure. The crystal structures and fluorescence-based thermal shift assays indicate that substituents larger than a methyl group are accommodated in the MbtI active site through significant but localized flexibility in the peptide backbone. These findings have implications for the design of improved inhibitors of MbtI, as well as other chorismate-utilizing enzymes from this family.

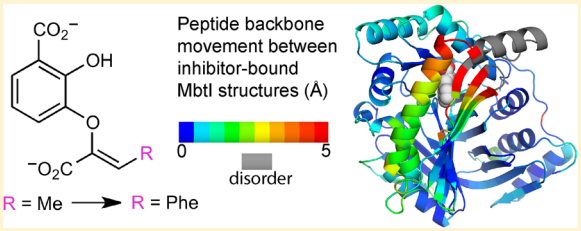

Tuberculosis (TB) is a lower-respiratory tract infection caused by *Mycobacterium tuberculosis*, from which more than 1.4 million people died in 2010.[1] The main therapeutic strategy to combat the disease relies on the administration of multiple drugs over ≥6 months,[2] which poses challenges in terms of patient compliance and the logistics of administration. These challenges are especially acute in the developing world, where the burden of disease is also the greatest. Multidrug-resistant (MDR) strains of *M. tuberculosis* are a growing problem,[3] and effective new antibiotics with novel modes of action are urgently required.[4,5]

Iron is a limiting nutrient for most pathogenic bacteria, and the pathways required for its acquisition are therefore potential targets for antibacterial development.[6] *M. tuberculosis* acquires iron using two pathways: chelating iron from the host using the siderophore mycobactin[7] and degrading heme released by damaged red blood cells.[8] The mycobactin-dependent pathway is required for the survival of *M. tuberculosis* under iron-deficient conditions in vitro, as well as in the macrophage.[9]

Mycobactin is a peptide-based siderophore synthesized by proteins encoded by the *mbt* and *mbt2* gene clusters.[10,11] Thus far, efforts to inhibit mycobactin biosynthesis have mainly focused on the first two enzymes from the mycobactin biosynthesis pathway, MbtI and MbtA.[12−20] MbtI is a salicylate synthase; it converts chorismate to salicylate via the intermediate isochorismate (Figure 1).[21] It is one of a family of chorismate-utilizing enzymes (CUEs) that share structural and mechanistic homology.[22] Enzymes from this family are present across the kingdoms of life, but absent in higher-order animals, and are involved in the biosynthesis of a number of important metabolites, including the aromatic amino acids, folate, menaquinones, and ubiquinones as well as siderophores (Figure 2).[23] Many members of this CUE family are attractive antibacterial targets, and several have been structurally characterized, including *Salmonella typhimurium* and *Serratia marcescens* anthranilate synthase (TrpE/TrpG),[24,25] *Escherichia coli* 4-amino-4-deoxychorismate synthase (PabB),[26] two *E. coli*

Received: February 15, 2012
Revised: April 24, 2012
Published: May 18, 2012

   dx.doi.org/10.1021/bi3002067 | *Biochemistry* 2012, 51, 4868−4879

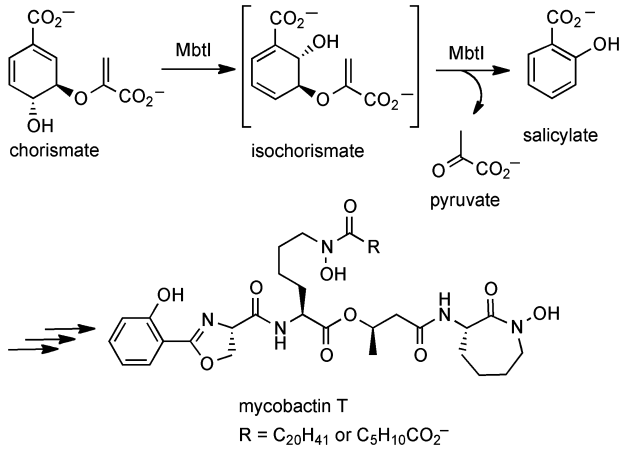

Figure 1. Reaction catalyzed by MbtI on the mycobactin biosynthesis pathway and the structure of mycobactin T.

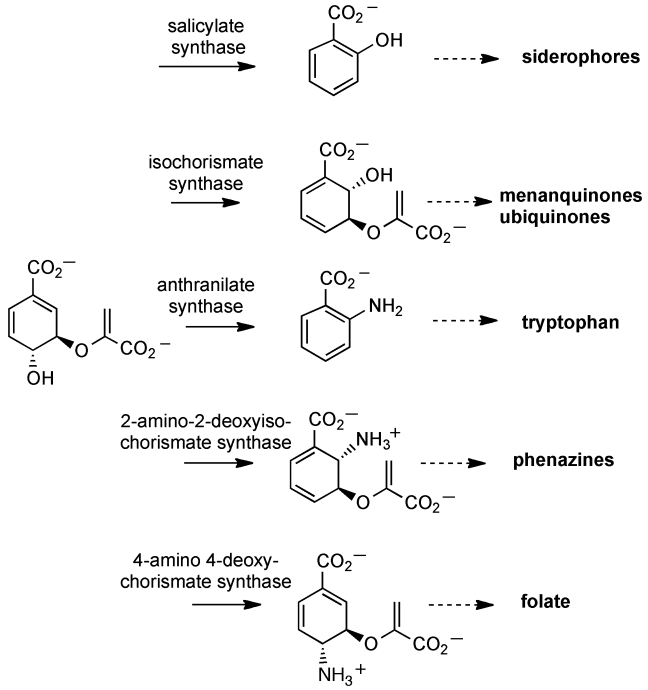

Figure 2. Reactions catalyzed by the chorismate-utilizing enzyme family, of which MbtI is a member.

isochorismate synthases (MenF and EntC),[27,28] *Yersinia enterocolitica* salicylate synthase (Irp9),[29] and MbtI.[21,30]

The earliest work on developing inhibitors of CUEs focused on mimics of chorismate, and putative intermediates and transition states in the reactions catalyzed by these enzymes.[31,32] The most potent compound synthesized to date is a putative transition state mimic with an inhibition constant (K_i) of 53 nM against *E. coli* EntC.[32] Subsequent studies have largely focused on more synthetically tractable aromatic mimics of chorismate, leading to the production of inhibitors of various CUEs with K_i values in the low micromolar range.[12,33−37] Recently, high-throughput methods have been utilized to identify more chemically diverse inhibitors of CUEs, again with the most potent compounds having K_i values in the low micromolar range.[13,38] Despite interest in the development of CUE inhibitors, thus far there is no detailed structural information about how these inhibitors bind to their target enzymes.

We recently reported a series of MbtI inhibitors based on an aromatic scaffold.[12] The most potent of these were mimics of isochorismate with hydrophobic substituents on the terminal alkene of the enolpyruvyl side chain (Figure 3). The

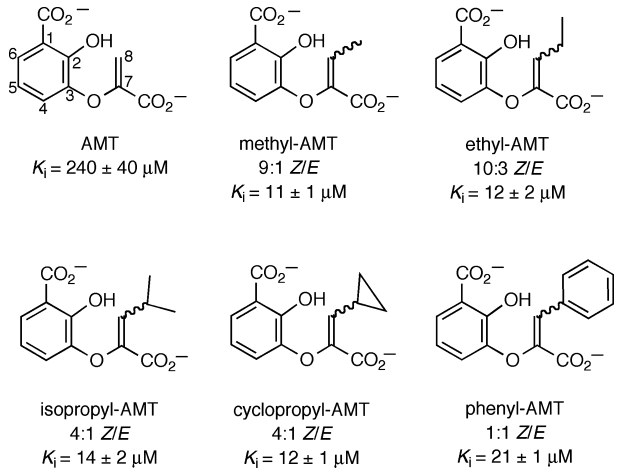

Figure 3. Inhibitors from the AMT series of isochorismate mimics for which cocrystal structures with MbtI were determined in this study. The molar ratio of *Z* and *E* isomers present in the diastereomeric mixture used for crystallography is given where applicable. K_i values against MbtI are as previously reported,[12] excluding the K_i for cyclopropyl-AMT which was determined as part of this study. The atom numbering scheme for these compounds is indicated on AMT.

substituents appended to the enolpyruvyl side chain varied in size from a methyl to a phenyl group. However, all these inhibitors exhibited potency an order of magnitude higher than that of the parental compound AMT, which carries a native enolpyruvyl side chain. Inhibitors from this series were designed on the basis of in silico molecular docking into a crystal structure of MbtI.[12] The in silico studies indicated that these inhibitors bind to MbtI in a manner analogous to that observed in crystal structures of other CUEs with reaction intermediates or products bound at the active site.[24,28,29,39] Here we report the first cocrystal structures of MbtI with inhibitors bound. Specifically, we report six crystal structures with inhibitors from our AMT series of isochorismate mimics bound to the active site of MbtI. This has allowed the binding modes for these inhibitors to be examined and the trends in their potency against MbtI to be rationalized. The results presented here provide important information for the future design of MbtI inhibitors, as well as inhibitors of other members of the CUE family.

MATERIALS AND METHODS

Protein Expression and Purification. MbtI was expressed with an N-terminal GST tag and initially purified as described previously.[12,21] After purification on glutathione Sepharose and removal of the GST tag as reported, the following additional purification steps were taken. MbtI was dialyzed into buffer A, consisting of 20 mM HEPES (pH 8.0), 2 mM $MgCl_2$, and 2 mM dithiothreitol (DTT). Anion exchange chromatography was conducted on a MonoQ HR 5/5 column (GE Healthcare) using an ionic strength gradient (20 mM to 1 M NaCl in buffer A over 60 column volumes) for protein elution. MbtI eluted at approximately 150−180 mM NaCl. Fractions containing MbtI

dx.doi.org/10.1021/bi3002067 | *Biochemistry* 2012, 51, 4868−4879

Table 1. Conditions for Crystallization of MbtI−Inhibitor Complexes

inhibitor	AMT	methyl-AMT	ethyl-AMT	cyclopropyl-AMT	isopropyl-AMT	phenyl-AMT
precipitant	17% PEG 6000, 0.2 M malic acid/KOH (pH 5.7)	15% PEG 4000, 0.2 M potassium thiocyanate	14% PEG 6000, 0.2 M malic acid/KOH (pH 5.5)	16% PEG 6000, 0.2 M malic acid/KOH (pH 5.5)	12% PEG 6000, 0.2 M malic acid/KOH (pH 5.5)	1.3 M $MgSO_4$, 0.13 M MES (pH 6.3)

were combined and concentrated to 15 mg/mL. The protein was further purified using size exclusion chromatography on a Superdex 200 16/60 size exclusion column (GE Healthcare) run with buffer A at a rate of 1 mL/min. Purified MbtI was concentrated to 25 mg/mL, flash-frozen in liquid nitrogen, and stored at 193 K.

Preparation and Characterization of Inhibitors. The synthesis of inhibitors, excluding cyclopropyl-AMT, was described previously.[12] The synthesis and characterization of cyclopropyl-AMT are described in the Supporting Information. Where applicable, inhibitors were used as a mixture of *E* and *Z* diastereomers as detailed in Figure 3. All inhibitors used in this study are listed below with the abbreviations for each and the relevant compound number from our previous report:[12] 3-(1-carboxyethenyloxy)-2-hydroxybenzoic acid (AMT, compound **38**), 3-(1-carboxyprop-1-enyloxy)-2-hydroxybenzoic acid (methyl-AMT, compound **39**), 3-(1-carboxybut-1-enyloxy)-2-hydroxybenzoic acid (ethyl-AMT, compound **41**), 3-(1-carboxy-2-cyclopropylethenyloxy)-2-hydroxybenzoic acid (cyclopropyl-AMT), 3-(1-carboxy-3-methylbut-1-enyloxy)-2-hydroxybenzoic acid (isopropyl-AMT, compound **40**), and 3-(1-carboxy-2-phenylvinyloxy)-2-hydroxybenzoic acid (phenyl-AMT, compound **42**).

Protein Crystallization. MbtI was cocrystallized with inhibitors from the AMT series by vapor diffusion in sitting drops. Drops consisted of 2 μL of 25 mg/mL MbtI and 2 μL of precipitant solution and were equilibrated at 292 K. Inhibitors were added to MbtI to a final concentration of 5 mM. The precipitant conditions used for crystallization of MbtI with each inhibitor are described in Table 1.

Data Collection and Processing for X-ray Crystallography. For data collection, crystals were soaked in a cryoprotectant solution consisting of the appropriate precipitant supplemented with 15% (v/v) glycerol. Crystals were subsequently flash-cooled to 110 K, and X-ray data were collected using a rotating anode X-ray source (Rigaku MicroMax-007, λ = 1.5418 Å) and a Mar345 image plate detector. For cocrystals of MbtI with the inhibitor AMT, data were collected using the MX1 and MX2 beamlines of the Australian Synchrotron (λ = 1.542 Å). For the cocrystal structure for *Z*-methyl-AMT, diffraction images were indexed and integrated with DENZO and scaled and merged using SCALEPACK in HKL-2000.[40] For all other inhibitor cocrystal structures, diffraction images were indexed and integrated using XDS[41] and scaled and merged using SCALA.[42] The data collection statistics for all crystals are listed in Table 2.

Structure Determination and Refinement for X-ray Crystallography. Structures were determined by molecular replacement with the apo structure of MbtI[21] (PDB entry 2G5F) as the search model. For the *Z*-methyl-AMT cocrystal structure, molecular replacement was conducted with MOLREP,[43] while all other structures were determined with Phaser_MR.[42] Several cycles of manual model building and refinement were conducted with COOT version 0.6[44] and either REFMAC5 version 5.5.0109[45,46] (*Z*-methyl-AMT structure) or Buster[47] (all other structures). The three-dimensional starting models of the inhibitors were generated and energy minimsed using the PRODRG server.[48] Automatic noncrystallographic symmetry restraints in Buster were used until the late stage of refinement. Water molecules were included in the model once R_{free} dropped below 0.3. Final models were assessed using Molprobity.[49] Refinement statistics are listed in Table 2. Figures of MbtI−inhibitor structures were generated with PyMOL.[50]

Structural Alignments. For each MbtI−inhibitor structure, the most well-defined MbtI molecule was chosen from the asymmetric unit to use in structural alignments. Structures were aligned in a pairwise fashion using equivalent Cα atoms from residues 20−449 or, when there was disorder in the structure, using those atoms from this residue range that could be modeled. Alignments were conducted, and rmsds between Cα atom positions were determined using LSQKAB.[51]

Fluorescence-Based Thermal Shift Assay. The thermal stability of MbtI in the absence and presence of inhibitors was measured using a fluorescence-based thermal shift assay. Aliquots (20 μL) of MbtI at 4 μM were combined with 2.5 μL of SYPRO Orange (Bio Rad) and 2.5 μL of buffer A or 2.5 μL of 10 mM inhbitor, to give a final inhibitor concentration of 1 mM. Triplicate samples were sealed in an iCycler-iQTM 96-well polymerase chain reaction (PCR) plate (Bio-Rad), and a thermal melt was conducted from 25 to 95 at 1 °C/min on a MyiQ Single color Real-Time PCR Detection System (Bio-Rad). The fluorescence intensity (excitation wavelength of 492 nm and emission wavelength of 610 nm) was monitored at each temperature, and the resulting thermal unfolding curves were fit to the Boltzmann equation using GraphPad Prism version 5.03 (GraphPad) to obtain the midpoint temperature for unfolding (T_m).[52] The change in T_m (ΔT_m) of MbtI resulting from the presence of each inhibitor was determined relative to the T_m of MbtI in the absence of inhibitor (52.7 ± 0.3 °C).

Solution State Conformation Calculations on AMT Series Inhibitors. Calculations for examination of the conformational landscapes of AMT, *Z*-methyl-AMT, and *E*-methyl-AMT were performed using the Gaussian09 software suite (revision C.01).[53] Density functional theory geometry optimization and surface scan calculations were conducted using the B3LYP hybrid functional[54,55] and the 6-31+G(d) basis set. The wave function was found to be stable under these conditions. Similar model chemistries involving double-ζ polar diffuse basis sets have been successfully employed for the analysis of enol pyruvate anions.[56] The effect of the solvent on the conformer geometry in water (H_2O; ε = 78.36) was simulated using the IEFPCM solvent model.[57] Harmonic vibrational analysis, at the same B3LYP/6-31+G(d) level, provided thermodynamic data and was used to determine the nature of the stationary points, i.e., no imaginary frequencies. Throughout these calculations, we assumed that the phenolic proton was hydrogen bonded to the C1 carboxylate moiety and that the carboxylates were deprotonated. Both mirror image structures and methyl group rotomers were eliminated during conformer searches. Methyl group rotomers were presumed to

Table 2. Data Collection and Refinement Statistics

	AMT	methyl-AMT	ethyl-AMT	cyclopropyl-AMT	isopropyl-AMT	phenyl-AMT
PDB entry	3ST6	3VEH	3RV9	3RV8	3RV7	3RV6
resolution range, (Å)[a]	29.4−1.75 (1.84−1.75)	47.3−2.00 (2.05−2.00)	19.8−2.30 (2.42−2.30)	19.7−2.29 (2.41−2.29)	19.8−2.50 (2.64−2.50)	19.6−2.04 (2.15−2.04)
space group	$P2_1$	$P2_1$	$P2_1$	$P2_1$	$P2_1$	$P2_1$
unit cell dimensions						
a (Å)	88.1	87.7	87.3	87.2	86.7	52.7
b (Å)	115.9	116.0	115.5	115.9	113.9	91.5
c (Å)	94.9	94.7	95.5	95.9	95.2	96.5
β (deg)	91.3	91.6	91.3	91.4	91.4	104.8
no. of molecules in the asymmetric unit	4	4	4	4	4	2
no. of unique reflections	187456	121077	83377	84681	63720	54595
multiplicity[a]	7.5 (7.2)	7.2 (5.7)	3.8 (3.7)	3.7 (3.4)	3.8 (3.8)	4.6 (4.3)
completeness (%)[a]	98.1 (97.0)	99.7 (98.9)	99.3 (98.7)	97.3 (91.9)	99.6 (99.3)	96.4 (90.6)
mean $I/\sigma(I)$[a]	12.1 (1.9)	15.8 (2.4)	12.8 (2.0)	11.4 (1.9)	12.7 (2.4)	21.0 (4.7)
R_{meas}[a,b]	0.076 (0.920)	0.070 (0.318)	0.114 (0.855)	0.100 (0.611)	0.108 (0.707)	0.068 (0.356)
R_{work}/R_{free}[c]	0.240/0.266	0.176/0.236	0.244/0.266	0.233/0.252	0.224/0.240	0.162/0.226
no. of non-hydrogen atoms						
protein	12810	13468	12692	12734	12820	6260
ligand	32	117	72	76	76	117
solvent	1002	981	315	318	457	628
average *B* factor						
main chain atoms	29.7	27.5	39.6	40.6	40.9	25.7
side chain atoms	35.1	31.1	44.7	44.5	45.8	31.1
waters	36.1	36.0	38.8	36.2	40.8	37.7
inhibitor	25.6	27.3	42.0	37.0	35.5	38.4
rmsd from ideal geometry						
bonds (Å)	0.015	0.023	0.013	0.031	0.032	0.015
angles (deg)	1.6	1.9	1.6	1.7	1.7	1.6

[a]Values in parentheses are for the outermost resolution shell. [b]For the definition of R_{meas}, see ref 62. [c]R_{work} and $R_{free} = \sum||F_{obs}| - |F_{calc}||/\sum|F_{obs}|$, where R_{free} was calculated with a randomly selected 5% of data not used in refinement.

dx.doi.org/10.1021/bi3002067 | *Biochemistry* 2012, 51, 4868−4879

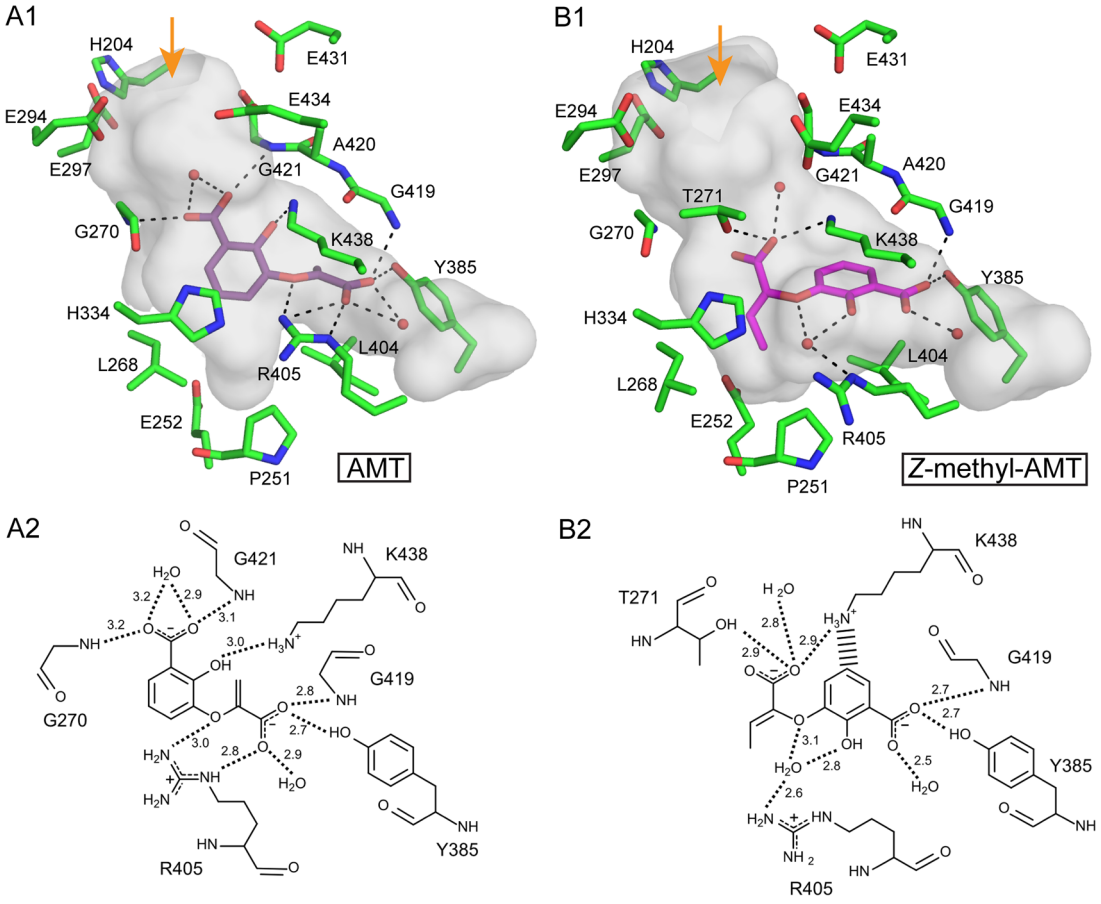

Figure 4. Two binding modes observed for AMT series inhibitors at the MbtI active site. AMT binds in mode 1 (A), while *Z*-methyl-AMT (B) binds in mode 2. (A1 and B1) Structures of AMT (purple) and *Z*-methyl-AMT (magenta), respectively, bound to MbtI. Gray shading indicates the surface of the active site cavity, and selected active site residues are shown. (A2 and B2) Two-dimensional schematic views of the interactions formed between selected active site residues of MbtI and AMT or *Z*-methyl-AMT, respectively. Hydrogen bonds are shown as dotted lines, with distances marked in angstroms. The cation–π interaction between K438 and *Z*-methyl-AMT is shown with broad dashes. An orange arrow indicates the entrance to the active site cavity in each case.

be present in both the protein-bound and free forms and would therefore have little effect on the relative conformation entropy of the three ligands. Only the more stable staggered methyl configurations were retained in conformer searches.

RESULTS AND DISCUSSION

General Features of Inhibitor-Bound MbtI Structures. Crystal structures were determined for MbtI bound to the inhibitor compounds AMT and methyl-, ethyl-, isopropyl-, cyclopropyl-, and phenyl-AMT at resolutions ranging from 1.8 to 2.5 Å (Tables 1 and 2). As was the case with inhibitor testing,[12] *E*/*Z* diastereomeric mixtures of compounds were used, where applicable. However, for all compounds except phenyl-AMT, only the *Z* isomer was observed bound to MbtI. Both the *E* and *Z* isomers of phenyl-AMT were observed, but bound to different MbtI molecules in the asymmetric unit. Overall, the crystal structures of inhibitor-bound MbtI obtained in this study are similar in conformation to those determined previously without added ligands,[12,21,30] with 21 β-strands folded into a twisted β-sandwich forming the core of the protein, surrounded by 10 α-helices. Consistent with previous structures, electron density is generally not observed for the 14 N-terminal residues in the inhibitor-bound structures because of disorder.

As a reference for comparing the inhibitor-bound structures, we use our previously most ordered MbtI structure, in which the active site adopts a fully closed conformation (PDB entry 3LOG).[12] In this structure, there is clear electron density for two molecules at the active site, which were modeled as carbonate and succinate ions. In addition, a monovalent cation is bound at the metal binding site detailed below, closing the entrance to the active site. This structure was the basis for in silico docking of compounds to MbtI during inhibitor development and will be subsequently termed the "closed form" of MbtI.

Structural superpositions of equivalent Cα atoms (residues 20–449) were conducted between the inhibitor-bound structures of MbtI and the closed form of MbtI (Figure S1 of the Supporting Information). This shows that for AMT-bound and *Z*-methyl-AMT-bound MbtI, the peptide backbone is in a conformation similar to that of the closed form, with rmsds between the structures of 0.9 and 0.6 Å, respectively. For the remaining inhibitors, there are more significant changes to the peptide backbone in regions proximal to the active site, including residues 268–293 and 324–336. The degree of movement in these regions generally increases as the size of the substituent on the inhibitor enolpyruvyl group increases, and in some cases, the electron density for residues in this region is either weak or not observed (Figure S2 of the Supporting

dx.doi.org/10.1021/bi3002067 | *Biochemistry* 2012, 51, 4868–4879

Information). Relative to the closed form of MbtI, the rmsds for equivalent Cα atoms (residues 20−450) are 1.0, 1.1, 1.6, 1.7, and 1.5 Å for *Z*-ethyl-, *Z*-isopropyl-, *Z*-cyclopropyl-, *Z*-phenyl-, and *E*-phenyl-AMT, respectively. However, the atomic positions of some residues in the flexible regions vary more significantly, with observed shifts of up to 10 Å. Disorder in these regions was also observed in two previous crystal structures of MbtI in which the active site adopts an open conformation.[21,30] The basis for structural perturbation in these regions is discussed in more detail below.

AMT Series Inhibitors Have Two Different Binding Modes. Two substantially different modes of binding of inhibitors to MbtI are observed (Figure 4). Mode 1 is similar to that expected for the binding of the reaction intermediate isochorismate, with the C1 carboxylate of the inhibitor oriented toward the metal binding site of the enzyme and the enolpyruvyl carboxylate interacting with an arginine residue (Arg405) deep in the active site. This binding mode is analogous to that previously observed in X-ray structures of CUEs with reaction products bound.[24,28,29,39] During MbtI inhibitor development, we predicted a similar binding mode for our series of aromatic isochorismate analogues based on in silico molecular docking to the closed form of MbtI.[12] The design of higher-potency inhibitors was undertaken using binding mode 1 as a framework.

Surprisingly, the MbtI−inhibitor crystal structures reveal that binding mode 1 is observed for only the least potent isochorismate analogue of the series, AMT (K_i = 240 μM), which has an unmodified enolpyruvyl side chain (Figure 4A). The remaining isochorismate analogues (methyl-, ethyl-, isopropyl-, cyclopropyl-, and phenyl-AMT), which carry substituents on the enolpyruvyl group, all utilize a novel binding mode, here termed mode 2 (Figure 4B). This correlates with the finding that these substituted AMT series inhibitors have potencies an order of magnitude higher than that of AMT (K_i = 11−21 μM). Mode 2 involves a complete reorientation of the isochorismate analogues within the active site. As described in detail below, for some inhibitors, movement of the peptide backbone away from the closed form of MbtI is necessary for binding in this mode.

AMT Binds to MbtI in Isochorismate-like Mode 1. AMT is the only inhibitor from the series for which the observed mode of binding to MbtI is similar to that predicted in our previous molecular docking studies,[12] i.e., mode 1 binding (Figure 4A). The structure shows clear electron density for the AMT inhibitor at the active sites of two MbtI molecules of the four in the asymmetric unit (Figure S3 of the Supporting Information). In the active sites of the two remaining MbtI molecules, there is relatively weak electron density for a bound ligand, but it is not of sufficient quality to unambiguously interpret as AMT.

Positioning of the active site residues in the MbtI−AMT complex is highly similar to that of the closed form of MbtI,[12] with a rmsd of 1.1 Å over all equivalent atoms in residues 20−449. The most significant variation occurs around the Mg^{2+} binding site, which is formed by the carboxylate side chains of Glu294, Glu297, Glu431, and Glu434 at the entrance to the MbtI active site. In the closed MbtI structure (PDB entry 3LOG), a sodium ion was modeled bound to this site; for the purpose of in silico docking, the expected native Mg^{2+} ion was substituted in its place and was predicted to interact with the C1 carboxylate of AMT. In the experimentally determined AMT-bound MbtI structure, the C1 carboxylate of AMT is oriented toward this site, but there is no metal ion evident in the structure, despite the presence of Mg^{2+} in the crystallization conditions. The metal binding site is not fully formed, with the side chain of Glu297 moved out of the active site and hydrogen bonded to the side chain of His204.

Instead of the predicted metal ion interaction, the C1 carboxylate of AMT is hydrogen bonded to the backbone amides of Gly270 and Gly421 and to an ordered water molecule near the metal binding site (Figure 4A). The C2 hydroxyl is within hydrogen bonding distance of Lys438. The enolpyruvyl group of the inhibitor is locked into a tight network of interactions in a binding pocket formed by the side chains of Arg405 and Tyr385, the backbone amide of Gly419, and a well-ordered water molecule. A charge−charge interaction also occurs between the carboxylate of the enolpyruvyl side chain and Arg405.

***Z*-Methyl-AMT Binds to MbtI in Mode 2.** Methyl-AMT is the most potent variant of the AMT series (K_i = 11 μM),[12] and as for all inhibitors carrying a substitutent on the enolpyruvyl side chain, this compound is observed to bind to MbtI in mode 2. Clear electron density is seen for methyl-AMT bound in the active site of each of the four MbtI molecules in the asymmetric unit (Figure S3 of the Supporting Information). In each case, the electron density is consistent with the *Z* isomer of methyl-AMT and was modeled as such. The *Z*-methyl-AMT-bound MbtI crystal structure will be used to illustrate the features of mode 2 binding.

Relative to the binding mode predicted by in silico studies, and the mode 1 binding observed for AMT, the orientation of *Z*-methyl-AMT is rotated by approximately 180° (Figure 4B). The 2-hydroxybenzoate ring of *Z*-methyl-AMT occupies the enolpyruvyl-binding pocket described for the AMT-bound MbtI structure, whereas the enolpyruvyl group of *Z*-methyl-AMT is oriented toward the opening of the active site. The intramolecular conformation of *Z*-methyl-AMT when bound to MbtI is also different from that of AMT, with a significant rotation of the enolpyruvyl group relative to the plane of the hydroxybenzoate ring. *Z*-Methyl-AMT bound to MbtI has C2−C3−O3−C7 and C3−O3−C7−C8 dihedral angles that are rotated 115° and 102°, respectively, relative to AMT bound to MbtI (see Figure 1 for atom numbering). The significance of this conformational change for the binding mode is explored in the computational analysis described below.

Overall, the conformations of active site residues are very similar in the AMT- and *Z*-methyl-AMT-bound MbtI structures. Arg405 is the only active site residue that undergos significant movement between the AMT and *Z*-methyl-AMT structures, with the side chain shifting by approximately 4 Å (Figure 4). This opens up a space that accommodates the 2-hydroxybenzoate ring of *Z*-methyl-AMT. Because the in silico molecular docking originally used to model the binding of AMT series inhibitors considers the protein structure as fixed,[12] it could not have predicted binding of *Z*-methyl-AMT in this position without flexibility being specifically permitted in the side chain position of Arg405. As for the AMT-bound structure, there is no metal ion at the active site entrance in the *Z*-methyl-AMT-bound structure, with the carboxylate side chain of Glu297 moving away from the metal binding site and forming a hydrogen bond with His204.

The C1 carboxylate of *Z*-methyl-AMT hydrogen bonds with Tyr385, the backbone amide of Gly419, and an ordered water molecule, in a manner analogous to that of the enolpyruvyl carboxylate of AMT (Figure 4B). An ordered water molecule

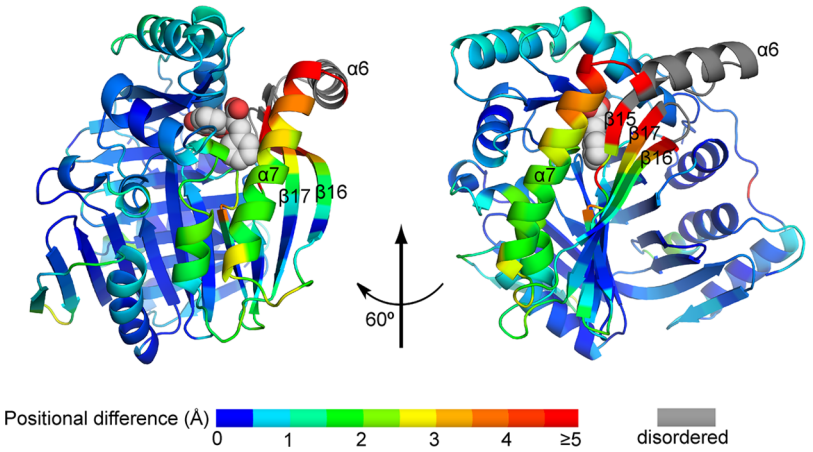

Figure 5. Positional differences (angstroms) between equivalent Cα atoms in the MbtI crystal structures with *Z*-phenyl- and *Z*-methyl-AMT bound, after global alignment of the two structures. The cartoon shows the structure determined for MbtI with *Z*-methyl-AMT bound, but with this inhibitor removed and *Z*-phenyl-AMT overlaid in its place as a space-filling model. Colors indicate the regions of the MbtI backbone that shift upon binding of *Z*-phenyl-AMT relative to the *Z*-methyl-AMT structure. Regions of the *Z*-phenyl-AMT structure that could not be modeled because of disorder are colored gray.

mediates hydrogen bonding of Arg405 and His334 with the 2-hydroxyl and enol oxygens of *Z*-methyl-AMT, respectively. The plane of the *Z*-methyl-AMT 2-hydroxybenzoate ring is sandwiched between the hydrophobic side chains of Leu404 and Lys438. A cation$-\pi$ interaction occurs with Lys438, with its side chain ε-amine positioned 3.4 Å above the center of the 2-hydroxybenzoate ring. The ε-amine of Lys438 also hydrogen bonds with the enolpyruvyl carboxylate of *Z*-methyl-AMT, which is further hydrogen bonded to the hydroxyl group of Thr271.

***Z*-Ethyl-, *Z*-Isopropyl-, *Z*-Cyclopropyl-, *Z*-Phenyl-, and *E*-Phenyl-AMT Are Accommodated through Localized Flexibility in the MbtI Active Site.** Crystal structures of the remaining AMT series inhibitors bound to MbtI show that all bind in mode 2. It was not evident from inspection of the *Z*-methyl-AMT structure that all the AMT derivatives would be able to bind in mode 2, as the methyl substituent sits in a constrained pocket with only 3.5−5 Å clearance. Hence, it appeared that inhibitors carrying larger substituents on the enolpyruvyl side chain would not readily fit in this binding mode. The structures determined here show that MbtI active site plasticity is the main factor allowing larger inhibitors to bind in this mode, but that moderate variations in inhibitor location at the active site and the internal conformation of each inhibitor also contribute.

Cocrystal structures of MbtI with ethyl-, isopropyl-, and cyclopropyl-AMT (K_i = 12−14 μM) show these compounds bound to all four molecules in the asymmetric unit, and the electron density is best modeled as the *Z* isomer (Figure S3 of the Supporting Information). However, the electron density for the terminal methyl groups of the ethyl and isopropyl compounds is weak, suggesting that these groups are able to rotate. There is no evidence in the electron density of the bound *E* isomer for these inhibitors. In contrast, in the cocrystal structure of MbtI with phenyl-AMT (K_i = 21 μM), there are only two molecules of MbtI in the asymmetric unit and both isomers of phenyl-AMT are present. There is clear electron density for the *Z* isomer of phenyl-AMT in the active site of one MbtI molecule and the *E* isomer in the active site of the second MbtI molecule (Figure S3 of the Supporting Information). In addition, *Z*-phenyl-AMT is observed bound at three other locations outside the active site, but these binding sites appear to be nonspecific and may result from the hydrophobic nature of this compound.

The most significant differences between the MbtI structure with *Z*-methyl-AMT bound and those with *Z*-ethyl-, *Z*-isopropyl- *Z*-cyclopropyl-, *Z*-phenyl-, and *E*-phenyl-AMT bound exist in regions proximal to the enolpyruvyl group comprising residues 268−293 and 324−336 (Figure 5 and Figures S1 and S2 of the Supporting Information). Electron density is weak or unobservable for some residues in this region, and shifts in the peptide backbone of up to 10 Å occur, relative to the closed form of MbtI. The flexible region encompasses a three-stranded β-sheet consisting of β-strands 15−17, which runs immediately alongside the enolpyruvyl-binding site and is shifted out from the active site to accommodate the bulkier substituents. Movement of this β-sheet propagates through the peptide backbone to cause disorder in α-helix 6, the N-terminus of α-helix 7, and intervening loop regions (Figure 5). Smaller changes are observed in other helices on the periphery of the MbtI structure, whereas the core β-sheet sandwich remains relatively invariant between structures

Structural changes and disorder that occur in these inhibitor-bound MbtI structures appear to originate from movements in active site residues immediately surrounding the enolpruvyl group. Leu268, Thr271, and His334 are located on β-strands 15 and 17 that line the enolpyruvyl binding site and sit on either end of the region of greatest perturbation (Figures 4B and 5). In the *Z*-methyl-AMT-bound MbtI structure, Leu268, Thr271, and His334 are positioned just 3.9, 2.7, and 3.6 Å, respectively, from the enolpyruvyl side chain. Ethyl, isopropyl, and cyclopropyl substituents on the enolpyruvyl side chain are accommodated by outward shifts of these residues via movement of the MbtI peptide backbone on the order of 1.5−3 Å. Binding of both isomers of phenyl-AMT is associated with more substantial reorganization of the peptide backbone in this region. The phenyl ring of *Z*-phenyl-AMT is inserted into a binding pocket created by approximately 3 Å shifts in the positions of Glu252, Thr261, and Leu268, all facilitated by peptide backbone movement. A cavity is created for the phenyl substituent of *E*-phenyl-AMT by an approximately 4 Å outward

dx.doi.org/10.1021/bi3002067 | *Biochemistry* 2012, 51, 4868−4879

shift of the backbone in the region of Leu268−Thr271 on the β15 strand.

As noted previously, although Arg405 is situated in a relatively fixed section of the MbtI active site, the side chain of this residue is flexible and appears to adapt to inhibitor binding. This residue is observed to form a range of different interactions with the core AMT structure in the cocrystal complexes of the six inhibitors that bind in mode 2. In the *Z*-ethyl-, *Z*-isopropyl-, and *Z*-cyclopropyl-AMT structures, the side chain of Arg405 directly hydrogen bonds to the 2-hydroxyl and enol oxygens of these AMT derivatives, rather than through the indirect, water-mediated interaction seen with *Z*-methyl-AMT (Figure S3 of the Supporting Information). In the *Z*-phenyl-AMT structure, the ordered water that hydrogen bonds with the C1 carboxylate group in the other inhibitor-bound structures is absent. In its place is the guanidinium group of Arg405, with the side chain bending around by almost 180° to form a direct head-to-head charge interaction with the C1 carboxylate group (Figure S3 of the Supporting Information). The *E*-phenyl-AMT-bound MbtI structure indicates no interaction between the inhibitor and Arg405.

Changes in active site placement of the larger inhibitors, relative to *Z*-methyl-AMT, also assist in weakening potentially unfavorable steric interactions. To compare the locations of the five larger substituted inhibitors in the MbtI active site with that of *Z*-methyl-AMT, we aligned the crystal structures using Tyr385 and Gly419 (Figure 4B and Figure S4 of the Supporting Information). These active site residues are relatively invariant in position between cocrystal structures and lock in the position of the C1 carboxylate of the inhibitors bound in mode 2. For *Z*-ethyl-, *Z*-isopropyl-, and *Z*-cyclopropyl-AMT, the location of the common AMT core structure of each inhibitor within the active site is very similar to that of *Z*-methyl-AMT, with rmsds of <1 Å. For the *Z* and *E* isomers of phenyl-AMT, the core 2-hydroxybenzoate ring also sits in a similar plane, sandwiched between Leu404 and Lys438. However, these inhibitors are displaced along this plane by 19° and 16°, respectively, relative to *Z*-methyl-AMT. This moves the phenyl substituents of both isomers into less constrained regions of the active site.

In addition, there are variations in the intramolecular conformation of the core AMT structure for these five inhibitors when bound to MbtI, compared to that observed for *Z*-methyl-AMT. This slightly alters the position of the enolpyruvyl group in relation to the relatively fixed position of the 2-hydroxybenzoate ring in the active site. The C2−C3−O3−C7 and C3−O3−C7−C8 dihedral angles of the core AMT structure for the larger substituted inhibitors vary by 20−36° and 9−27°, respectively, relative to those of *Z*-methyl-AMT. The greatest changes in these angles occur for *E*-phenyl-AMT.

As observed with the smaller inhibitors, there is no metal ion evident at the active site entrance in MbtI with *Z*-ethyl-, *Z*-isopropyl-, and *Z*-cyclopropyl-AMT bound. In the phenyl-AMT cocrystal structure, the electron density is consistent with Mg^{2+} ions at the metal binding site in both monomers in the asymmetric unit. These metal ions appear to be surrounded by a hydration shell, through which they interact with the glutamate residues that constitute the metal binding site. The *E*-phenyl-AMT structure is the only inhibitor-bound MbtI structure in which the side chain of Glu297 is in position to form the full metal binding site. Because the phenyl-AMT cocrystals were obtained in a precipitant containing 1.3 M $MgSO_4$, these hydrated Mg^{2+} ions may bind as an artifact of the very high metal ion concentration. There is no direct interaction between the metal ion and either *Z*-phenyl- or *E*-phenyl-AMT.

Active Site Flexibility Is Observed in Previously Determined Structures of MbtI. From a comparison with previously determined structures of MbtI in which the active site is in an open conformation[21,30] (PDB entries 2G5F and 2I6Y), it is clear that there is inherent flexibility in the regions of the MbtI structure that undergo changes upon binding of inhibitors larger than *Z*-methyl-AMT. The greatest peptide backbone variation between the closed structure of MbtI and the two open structures occurs across β-strands 15−17 and α-helix 6 (Figure S1 of the Supporting Information). In the structure determined by Zwahlen et al.[30] (PDB entry 2I6Y), in which there is no ligand bound at the active site, residues could not be modeled for sections of this β-sheet and α-helix because of disorder. In the open structure previously determined by us[21] (PDB entry 2G5F), which contains a pyruvate ion bound to the active site, the strands of the β-sheet move outward from the active site by up to 5 Å relative to the closed form of MbtI.

These observations suggest that the binding of inhibitors with an enolpyruvyl substituent larger than a methyl is not directly inducing movement and disorder in the MbtI peptide backbone. Rather, the inhibitors are sampling a preexisting conformation of MbtI that is readily accessible because of flexibility in these regions of the structure. This hypothesis is consistent with the modest decrease in inhibitor potency as the enolpyruvyl substituent size is increased from a methyl (K_i = 11 μM) to a phenyl group (K_i = 21 μM).[12]

Interestingly, against *S. marcescens* anthranilate synthase, a more significant loss of potency was observed as the size of the substituent was increased. Methyl-AMT, ethyl-AMT, cyclopropyl-AMT, and phenyl-AMT have K_i values of 1.1, 1.7, 5.0, and 34 μM, respectively, with the latter being equivalent to the unmodified parental AMT compound.[12] In contrast to MbtI, which is a monomer in solution, *S. marcescens* anthranilate synthase is a heterotetramer consisting of two TrpE−TrpG dimers, with the interface between the two dimers occurring between the TrpE subunits.[24] Overlaying the MbtI structure with the available crystal structure of this anthranilate synthase shows that the dimer interface occurs at the position equivalent to α-helix 6 of MbtI. It is this helix that becomes disordered in response to the binding of larger inhibitors to MbtI. Hence, the flexibility seen in the MbtI peptide backbone in this region is most likely not available in *S. marcescens* anthranilate synthase because of its quaternary structure, and this may explain why this enzyme is less tolerant than MbtI to larger inhibitor substituents.

Thermal Shift Assays Are Consistent with Larger AMT Series Inhibitors Binding a Disordered Form of MbtI. Fluorescence-based thermal shift assays of MbtI support the structure-based observation that inhibitors larger than methyl-AMT bind to a more disordered form of the enzyme. In principle, the interactions formed upon inhibitor binding should stabilize the folded form of MbtI in solution, causing an increase in the observed midpoint temperature for protein unfolding (T_m).[52] AMT series inhibitors were added to MbtI at saturating concentrations, and the change in T_m (ΔT_m) was determined relative to the T_m in the absence of an inhibitor. The ΔT_m value was used as an indicator of the degree of stabilization conferred by each inhibitor.

The results of the thermal shift assay show that the size of the substituent on the inhibitor enolpyruvyl group is negatively

Table 3. Fluorescence-Based Thermal Shift Assays of MbtI in the Presence of AMT Series Inhibitors

inhibitor	AMT	methyl-AMT	ethyl-AMT	cyclopropyl-AMT	isopropyl-AMT	phenyl-AMT
ΔT_m (°C)[a]	2.8 ± 0.4	8.3 ± 0.3	7.5 ± 0.3	7.3 ± 0.4	4.6 ± 0.5	1.2 ± 0.4
K_i (μM)	240 ± 40[b]	11 ± 1[b]	12 ± 2[b]	12 ± 1	14 ± 2[b]	21 ± 5[b]

[a]ΔT_m corresponds to the change in midpoint temperature for unfolding of MbtI in the presence of an inibitor relative to the T_m in the absence of an inhibitor. [b]Value from ref 12.

correlated with the degree of stabilization provided by the inhibitor (Table 3). The presence of saturating amounts of methyl-AMT considerably stabilizes the MbtI structure with an increase in the midpoint temperature for unfolding (ΔT_m) of 8.3 ± 0.3 °C relative to that of MbtI alone (Table 3). This is consistent with the highly ordered MbtI crystal structure observed with this inhibitor bound. As the size of the enolpyruvyl substituent of the inhibitor is increased, there is an incremental decrease in the observed level of stabilization of the MbtI structure, with the presence of phenyl-AMT producing a ΔT_m of only 1.2 ± 0.4 °C.

The fact that the K_i values for all of the substituted AMT inhibitors are similar in magnitude[12] suggests that all have similar binding affinity for MbtI. Hence, it is likely that this trend in ΔT_m is a reflection of the localized disorder upon binding of larger substituted inhibitors observed in the inhibitor-bound MbtI crystal structures. Our results indicate that, although inhibitors larger than methyl-AMT stabilize the structure of MbtI overall, resulting in an increase in T_m, these inhibitors appear to select a conformation of MbtI less tightly folded than that selected by methyl-AMT.

Computational Studies Indicate a Correlation of Binding Mode and Potency with the Conformational Landscape of Inhibitors in Solution. Insight into the switch in binding mode, and the higher potency, exhibited by inhibitors carrying a modified enolpyruvyl group was achieved by exploring the conformational landscape of the inhibitors. Solution phase global minimum structures were calculated for AMT, *E*-methyl-AMT, and *Z*-methyl-AMT and compared with the experimentally determined conformations when bound to MbtI. In addition, statistical conformational entropy (S_{conf}) values were estimated to examine if entropic factors contribute to the higher potency of methyl-AMT. For this analysis, we assumed that the inhibitors have very low conformational entropy when bound to the enzyme, thus allowing the ΔS_{conf} value for each inhibitor on formation of the protein−inhibitor complex to be estimated on the basis of solution state calculations on the unbound inhibitor. The changes in conformational entropy of the protein and solvent upon inhibitor binding were also not considered in our analysis but may have a significant effect on inhibitor potency.

Conformational landscapes of AMT, *E*-methyl-AMT, and *Z*-methyl-AMT were surveyed with respect to the two dihedral angles determining the position of the enolpyruvyl side chain relative to the 2-hydroxybenzoate ring: C3−O3−C7−C8 (D_1) and C2−C3−O3−C7 (D_2) (Figure 6 and Figure S5 of the Supporting Information). A systematic density functional theory approach was used to identify global minimum structures in solution. Conformer distributions were calculated for each inhibitor in three stages. First, the three-dimensional potential energy surfaces of D_1 and D_2 were mapped with 18° resolution (Figure S5 of the Supporting Information). Second, all minima identified were reoptimized without geometric constraint. Finally, the unscaled zero-point-corrected energies for all minimum confomers were calculated to give the

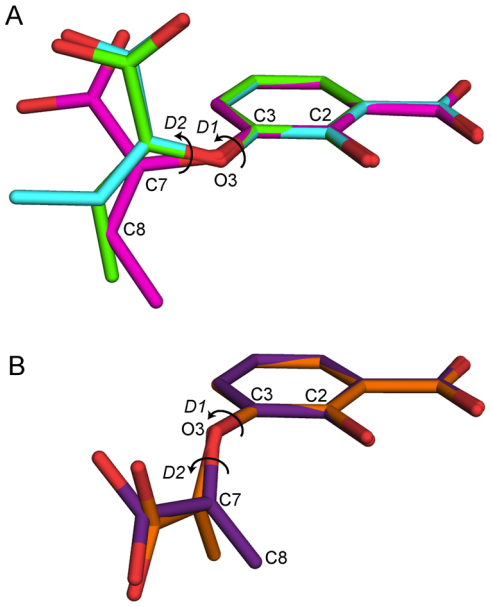

Figure 6. (A) Conformation of *Z*-methyl-AMT bound to MbtI (magenta) overlaid with calculated solution state global minimum conformations for *Z*-methyl-AMT (green) and *E*-methyl-AMT (cyan). (B) Conformation of AMT bound to MbtI (purple) overlaid with a calculated solution state global minimum conformation for AMT (orange).

Boltzmann populations and the overall conformational entropy of each inhibitor (Tables S1−S3 of the Supporting Information). It should be noted that for each conformational minimum found, a nonsuperimposable mirror image structure exists with equal energy.

Interestingly, for both *Z*-methyl-AMT and *E*-methyl-AMT, the solution state global minimum structures resemble the actual conformation of *Z*-methyl-AMT bound to MbtI (Table 4 and Figure 6). Dihedral angles D_1 and D_2 are −173° and 107°,

Table 4. Comparison between Dihedral Angles in MbtI-Bound and Calculated Solution State Global Minimum Structures of AMT Series Inhibitors

	experimental MbtI-bound conformation		calculated solution state global minimum conformation[a]	
	D_1[b] (deg)	D_2[b] (deg)	D_1[b] (deg)	D_2[b] (deg)
AMT	−58	5	−89	−2
E-methyl-AMT	na[c]	na[c]	162	126
Z-methyl-AMT	−173	107	163	117

[a]For each global minimum conformation listed here, a non-superimposable mirror image structure exists with equal energy. These have dihedral angles of the same magnitude but opposite sign compared to those listed. [b]D_1 corresponds to the C2−C3−O3−C7 dihedral angle. D_2 corresponds to the C3−O3−C7−C8 dihedral angle. [c]Structure of *E*-methyl-AMT bound to MbtI not determined.

dx.doi.org/10.1021/bi3002067 | *Biochemistry* 2012, 51, 4868−4879

respectively, in the experimental structure of *Z*-methyl-AMT bound to MbtI. D_1 and D_2 for the calculated minimum conformer of *Z*-methyl-AMT differ by 24° and 10°, respectively, from these angles. The results are similar for *E*-methyl-AMT with variations of 25° and 19° for D_1 and D_2, respectively, between the minimum conformation and the MbtI-bound *Z*-methyl-AMT structure. This suggests that in solution both *Z*-methyl-AMT and *E*-methyl-AMT are to some degree preorganized for binding to MbtI in a conformation similar to mode 2.

Correspondingly, for AMT there is a resemblance between the solution state global minimum structures and the experimentally determined conformation of AMT bound to MbtI (Table 4 and Figure 6). Dihedral angles D_1 and D_2 are −58° and 5°, respectively, for AMT in the MbtI-bound structure. The calculated global minimum conformer of AMT has D_1 and D_2 angles that differ by 33° and 7°, respectively, from those of this bound conformation. Therefore, the solution state conformation of AMT is closer to that required for binding in mode 1.

Calculations on the distribution of minima and overall solution state conformational entropy values (S_{conf}) for each inhibitor show that *Z*-methyl-AMT is the least disordered (Tables S1−S3 of the Supporting Information). The methyl substituent of *Z*-methyl-AMT effectively works as a conformational lock, disfavoring conformers in which the methyl group would sterically interact with the C2 hydroxyl group. Therefore, *Z*-methyl-AMT has the lowest S_{conf} of 0.8 J K^{-1} mol^{-1}, with the Boltzmann distribution indicating that 98% of the compound will exist in the conformations corresponding to the global minimum. AMT and *E*-methyl-AMT have higher S_{conf} values of 5.1 and 3.8 J K^{-1} mol^{-1}, respectively. Correspondingly, it is estimated that for AMT and *E*-methyl-AMT, 75 and 86% of each compound, respectively, will exist in the global minimum conformations.

On the basis of these calculations, and considering only the entropic cost of restricting the inhibitor structure upon formation of the MbtI−inhibitor complex, *Z*-methyl-AMT is expected to the most effective inhibitor. Unfortunately, in our previous study, the two isomers of methyl-AMT could not be entirely separated to conclusively determine which is more potent.[12] Diastereomeric mixtures of methyl-AMT containing predominantly the *Z* isomer (K_i = 11 μM) or the *E* isomer (K_i = 14 μM) show comparable inhibitor potency against MbtI. However, against the homologous enzyme, *S. marcescens* anthranilate synthase, a diastereomeric mixture containing predominantly the *Z* isomer (K_i = 1.1 μM) is an order of magnitude more potent than one consisting predominantly of the *E* isomer (K_i = 34 μM). It is also interesting to note that for the MbtI-bound crystal structures of all AMT derivatives, excluding that of phenyl-AMT, only the *Z* isomer is observed. However, this may simply reflect the higher concentration of the *Z* isomer in the diastereomeric mixtures used for cocrystallization with MbtI.[12]

CONCLUSION

The inhibitor-bound MbtI crystal structures determined in this study reveal a correlation of inhibitor potency with observed binding mode. It is evident that a subsitutent on C8 of the enolpyruvyl side chain of the core AMT compound leads to a switch in binding mode. The least potent compound of the series, AMT, binds in a substrate-like mode, close to that predicted for our inhibitor series from in silico modeling studies.[12] The higher-potency AMT variants, which carry hydrophobic substituents on the enolpyruvyl side chain, have a binding mode that is flipped by almost 180° relative to that of AMT. Computational studies suggest that this change in binding mode is due to modulation of the conformational landscape of the AMT core of the inhibitors upon addition of a substituent to the enolpyruvyl side chain. Considerable localized plasticity is observed in the MbtI active site and appears to be facilitated by inherent flexibility in the surrounding peptide backbone. This allows the larger inhibitors from the AMT series to be accommodated at the active site and is consistent with the tolerance of MbtI to various substituents on the enolpyruvyl side chain.

To the best of our knowledge, the MbtI structures obtained in this study are the first for this family of chorismate-utilizing enzymes that contain an inhibitor bound to the active site. Hence, these structures provide information that could be used to guide inhibitor development against other enzymes from this CUE family. More generally, our results emphasize the importance of considering conformational flexibility in both inhibitor compounds and target enzymes for inhibitor design.[58−61] On the basis of the structural information gained in this study, our future work will focus on elaborating the AMT series of MbtI inhibitors to both optimize the inhibitor conformation for binding and gain further inhibitor−protein interactions, with the ultimate aim of developing an anti-TB drug with a novel mode of action.

ASSOCIATED CONTENT

Supporting Information

Supplementary methods, including synthesis and testing of MbtI inhibitor cyclopropyl-AMT, positional differences between equivalent Cα atoms (angstroms) in each inhibitor-bound MbtI structure and a structure of MbtI with a closed and ordered active site (PDB entry 3LOG) (Figure S1), movement and disorder observed around the active site in cocrystal structures of MbtI with inhibitors (Figure S2), $2F_o - F_c$ omit maps for MbtI−inhibitor structures (Figure S3), comparison of active site positioning of *Z*-isopropyl-AMT and *Z*-phenyl-AMT with that of *Z*-methyl-AMT (Figure S4), graphs of solution state conformation calculations on AMT-series inhibitors (Figure S5), solution state conformation calculations on AMT (Table S1), solution state conformation calculations on *E*-methyl-AMT (Table S2), and solution state conformation calculations on *Z*-methyl-AMT (Table S3). This material is available free of charge via the Internet at http://pubs.acs.org.

Accession Codes

Atomic coordinates of enzyme−inhibitor complexes have been deposited in the Protein Data Bank as entries 3ST6, 3VEH, 3RV6, 3RV7, 3RV8, and 3RV9.

AUTHOR INFORMATION

Corresponding Author

*J.S.L.: e-mail, s.lott@auckland.ac.nz; phone, +64 9 3737599, ext. 87074. E.M.M.B.: e-mail, e.bulloch@auckland.ac.nz; phone, +64 9 3737599, ext. 82173.

Funding

This work was supported by funding from Health Research Council of New Zealand Programme Grant 09/110B, New Zealand Ministry of Science and Innovation New Economy Research Fund Contract UOAX1005, and the Maurice Wilkins Centre for Molecular Biodiscovery. E.M.M.B. has been

supported by a New Zealand Ministry of Science and Innovation postdoctoral fellowship and Subcontract 70218-001-08 from the National Institutes of Health via the *Mycobacterium tuberculosis* Structural Genomics Consortium.

Notes

The authors declare no competing financial interest.

■ ACKNOWLEDGMENTS

We thank Dr. Tet Verne Lee, Dr. Richard Bunker, and Jason Busby for valuable input into structure refinement and Dr. Richard Kingston for useful comments on the manuscript.

■ ABBREVIATIONS

MbtI, *M. tuberculosis* salicylate synthase; CUE, chorismate-utilizing enzyme; TrpE/TrpG, anthranilate synthase; PabB, 4-amino-4-deoxychorismate synthase; MenF and EntC, isochorismate synthase; K_i, inhibition constant; GST, glutathione *S*-transferase; HEPES, 4-(2-hydroxyethyl)-1-piperazineethanesulfonic acid; DTT, dithiothreitol; AMT, 3-(1-carboxyethenyloxy)-2-hydroxybenzoic acid; methyl-AMT, 3-(1-carboxyprop-1-enyloxy)-2-hydroxybenzoic acid; ethyl-AMT, 3-(1-carboxybut-1-enyloxy)-2-hydroxybenzoic acid; cyclopropyl-AMT, 3-(1-carboxy-2-cyclopropylethenyloxy)-2-hydroxybenzoic acid; isopropyl-AMT, 3-(1-carboxy-3-methylbut-1-enyloxy)-2-hydroxybenzoic acid; phenyl-AMT, 3-(1-carboxy-2-phenylvinyloxy)-2-hydroxybenzoic acid; T_m, midpoint unfolding temperature; B3LYP, Becke three-parameter hybrid functional with Lee−Yang−Parr correlation function; S_{conf}, conformational entropy; rmsd, root-mean-square deviation; PDB, Protein Data Bank.

■ REFERENCES

(1) World Health Organization (2012) Global Tuberculosis Control 2011.

(2) Iseman, M. (2002) Tuberculosis therapy: Past, present and future. *Eur. Respir. J. 20*, 87s−94s.

(3) World Health Organization (2010) Multidrug and extensively drug-resistant TB (M/XDR-TB): 2010 global report on surveillance and response.

(4) Koul, A., Arnoult, E., Lounis, N., Guillemont, J., and Andries, K. (2011) The challenge of new drug discovery for tuberculosis. *Nature 469*, 483−490.

(5) Ma, Z., Lienhardt, C., Mcilleron, H., Nunn, A. J., and Wang, X. (2010) Global tuberculosis drug development pipeline: The need and the reality. *Lancet 375*, 2100−2109.

(6) Schaible, U., and Kaufmann, S. (2004) Iron and microbial infection. *Nat. Rev. Microbiol. 2*, 946−953.

(7) De Voss, J. J., Rutter, K., Schroeder, B. G., and Barry, C. E. (1999) Iron acquisition and metabolism by mycobacteria. *J. Bacteriol. 181*, 4443−4451.

(8) Chim, N., Iniguez, A., Nguyen, T. Q., and Goulding, C. W. (2010) Unusual Diheme Conformation of the Heme-Degrading Protein from *Mycobacterium tuberculosis*. *J. Mol. Biol. 395*, 595−608.

(9) De Voss, J. J., Rutter, K., Schroeder, B. G., Su, H., Zhu, Y., and Barry, C. E. (2000) The salicylate-derived mycobactin siderophores of *Mycobacterium tuberculosis* are essential for growth in macrophages. *Proc. Natl. Acad. Sci. U.S.A. 97*, 1252−1257.

(10) Quadri, L. E., Sello, J., Keating, T. A., Weinreb, P. H., and Walsh, C. T. (1998) Identification of a *Mycobacterium tuberculosis* gene cluster encoding the biosynthetic enzymes for assembly of the virulence-conferring siderophore mycobactin. *Chem. Biol. 5*, 631−645.

(11) Frankel, B. A., and Blanchard, J. S. (2008) Mechanistic analysis of *Mycobacterium tuberculosis* Rv1347c, a lysine Nε-acyltransferase involved in mycobactin biosynthesis. *Arch. Biochem. Biophys. 477*, 259−266.

(12) Manos-Turvey, A., Bulloch, E., Rutledge, P., Baker, E., Lott, J., and Payne, R. (2010) Inhibition studies of *Mycobacterium tuberculosis* salicylate synthase (MbtI). *ChemMedChem 5*, 1067−1079.

(13) Vasan, M., Neres, J., Williams, J., Wilson, D. J., Teitelbaum, A. M., Remmel, R. P., and Aldrich, C. C. (2010) Inhibitors of the Salicylate Synthase (MbtI) from *Mycobacterium tuberculosis* Discovered by High-Throughput Screening. *ChemMedChem 5*, 2079−2087.

(14) Labello, N. P., Bennett, E. M., Ferguson, D. M., and Aldrich, C. C. (2008) Quantitative Three Dimensional Structure Linear Interaction Energy Model of 5′-O-[N-(Salicyl)sulfamoyl]adenosine and the Aryl Acid Adenylating Enzyme MbtA. *J. Med. Chem. 51*, 7154−7160.

(15) Neres, J., Labello, N. P., Somu, R. V., Boshoff, H. I., Wilson, D. J., Vannada, J., Chen, L., Barry, C. E., Bennett, E. M., and Aldrich, C. C. (2008) Inhibition of siderophore biosynthesis in *Mycobacterium tuberculosis* with nucleoside bisubstrate analogues: Structure-activity relationships of the nucleobase domain of 5′-O-[N-(salicyl)sulfamoyl]-adenosine. *J. Med. Chem. 51*, 5349−5370.

(16) Neres, J., Wilson, D. J., Celia, L., Beck, B. J., and Aldrich, C. C. (2008) Aryl acid adenylating enzymes involved in siderophore biosynthesis: Fluorescence polarization assay, ligand specificity, and discovery of non-nucleoside inhibitors via high-throughput screening. *Biochemistry 47*, 11735−11749.

(17) Qiao, C., Gupte, A., Boshoff, H. I., Wilson, D. J., Bennett, E. M., Somu, R. V., Barry, C. E., and Aldrich, C. C. (2007) 5′-O-[(N-Acyl)sulfamoyl]adenosines as antitubercular agents that inhibit MbtA: An adenylation enzyme required for siderophore biosynthesis of the mycobactins. *J. Med. Chem. 50*, 6080−6094.

(18) Somu, R. V., Wilson, D. J., Bennett, E. M., Boshoff, H. I., Celia, L., Beck, B. J., Barry, C. E., and Aldrich, C. C. (2006) Antitubercular nucleosides that inhibit siderophore biosynthesis: SAR of the glycosyl domain. *J. Med. Chem. 49*, 7623−7635.

(19) Vannada, J., Bennett, E. M., Wilson, D. J., Boshoff, H. I., Barry, C. E., and Aldrich, C. C. (2006) Design, synthesis, and biological evaluation of β-ketosulfonamide adenylation inhibitors as potential antitubercular agents. *Org. Lett. 8*, 4707−4710.

(20) Somu, R. V., Boshoff, H., Qiao, C., Bennett, E. M., Barry Iii, C. E., and Aldrich, C. C. (2006) Rationally-designed nucleoside antibiotics that inhibit siderophore biosynthesis of *Mycobacterium tuberculosis*. *J. Med. Chem. 49*, 31−34.

(21) Harrison, A. J., Yu, M., Gårdenborg, T., Middleditch, M., Ramsay, R. J., Baker, E. N., and Lott, J. S. (2006) The structure of MbtI from *Mycobacterium tuberculosis*, the first enzyme in the biosynthesis of the siderophore mycobactin, reveals it to be a salicylate synthase. *J. Bacteriol. 188*, 6081−6091.

(22) He, Z., Stigers Lavoie, K. D., Bartlett, P. A., and Toney, M. D. (2004) Conservation of mechanism in three chorismate-utilizing enzymes. *J. Am. Chem. Soc. 126*, 2378−2385.

(23) Dosselaere, F., and Vanderleyden, J. (2001) A metabolic node in action: Chorismate-utilizing enzymes in microorganisms. *Crit. Rev. Microbiol. 27*, 75−131.

(24) Spraggon, G., Kim, C., Nguyen-Huu, X., Yee, M. C., Yanofsky, C., and Mills, S. E. (2001) The structures of anthranilate synthase of *Serratia marcescens* crystallized in the presence of (i) its substrates, chorismate and glutamine, and a product glutamate, and (ii) its end-product inhibitor, L-tryptophan. *Proc. Natl. Acad. Sci. U.S.A. 98*, 6021−6026.

(25) Morollo, A. A., and Eck, M. J. (2001) Structure of the cooperative allosteric anthranilate synthase from *Salmonella typhimurium*. *Nat. Struct. Mol. Biol. 8*, 243−247.

(26) Parsons, J., Jensen, P., Pachikara, A., Howard, A., Eisenstein, E., and Ladner, J. (2002) Structure of *Escherichia coli* aminodeoxychorismate synthase: Architectural conservation and diversity in chorismate-utilizing enzymes. *Biochemistry 41*, 2198−2208.

(27) Kolappan, S., Zwahlen, J., Zhou, R., Truglio, J., Tonge, P., and Kisker, C. (2007) Lysine 190 is the catalytic base in MenF, the menaquinone-specific isochorismate synthase from *Escherichia coli*: Implications for an enzyme family. *Biochemistry 46*, 946−953.

(28) Sridharan, S., Howard, N., Kerbarh, O., Błaszczyk, M., Abell, C., and Blundell, T. L. (2010) Crystal structure of *Escherichia coli* enterobactin-specific isochorismate synthase (EntC) bound to its reaction product isochorismate: Implications for the enzyme mechanism and differential activity of chorismate-utilizing enzymes. *J. Mol. Biol. 397*, 290−300.
(29) Kerbarh, O., Chirgadze, D. Y., Blundell, T. L., and Abell, C. (2006) Crystal structures of *Yersinia enterocolitica* salicylate synthase and its complex with the reaction products salicylate and pyruvate. *J. Mol. Biol. 357*, 524−534.
(30) Zwahlen, J., Kolappan, S., Zhou, R., Kisker, C., and Tonge, P. (2007) Structure and mechanism of MbtI, the salicylate synthase from *Mycobacterium tuberculosis*. *Biochemistry 46*, 954−964.
(31) Walsh, C. T., Erion, M. D., Walts, A. E., Delany, J. J., and Berchtold, G. A. (1987) Chorismate Aminations: Partial-Purification of *Escherichia coli* PABA Synthase and Mechanistic Comparison with Anthranilate Synthase. *Biochemistry 26*, 4734−4745.
(32) Kozlowski, M., Tom, N., Seto, C., Sefler, A., and Bartlett, P. (1995) Chorismate-utilizing enzymes isochorismate synthase, anthranilate synthase, and *p*-aminobenzoate synthase: Mechanistic insight through inhibitor design. *J. Am. Chem. Soc. 117*, 2128−2140.
(33) Payne, R. J., Bulloch, E. M. M., Abell, A. D., and Abell, C. (2005) Design and synthesis of aromatic inhibitors of anthranilate synthase. *Org. Biomol. Chem. 3*, 3629−3635.
(34) Payne, R. J., Kerbarh, O., Miguel, R. N., Abell, A. D., and Abell, C. (2005) Inhibition studies on salicylate synthase. *Org. Biomol. Chem. 3*, 1825−1827.
(35) Payne, R. J., Bulloch, E. M. M., Toscano, M. M., Jones, M. A., Kerbarh, O., and Abell, C. (2009) Synthesis and evaluation of 2,5-dihydrochorismate analogues as inhibitors of the chorismate-utilising enzymes. *Org. Biomol. Chem. 7*, 2421−2429.
(36) Payne, R. J., Bulloch, E. M. M., Kerbarh, O., and Abell, C. (2010) Inhibition of chorismate-utilising enzymes by 2-amino-4-carboxypyridine and 4-carboxypyridone and 5-carboxypyridone analogues. *Org. Biomol. Chem. 8*, 3534−3542.
(37) Payne, R. J., Toscano, M. D., Bulloch, E. M. M., Abell, A. D., and Abell, C. (2005) Design and synthesis of aromatic inhibitors of anthranilate synthase. *Org. Biomol. Chem. 3*, 2271.
(38) Ziebart, K. T., Dixon, S. M., Avila, B., El-Badri, M. H., Guggenheim, K. G., Kurth, M. J., and Toney, M. D. (2010) Targeting multiple chorismate-utilizing enzymes with a single inhibitor: Validation of a three-stage design. *J. Med. Chem. 53*, 3718−3729.
(39) Li, Q. A., Mavrodi, D. V., Thomashow, L. S., Roessle, M., and Blankenfeldt, W. (2011) Ligand binding induces an ammonia channel in 2-amino-2-desoxyisochorismate (ADIC) synthase PhzE. *J. Biol. Chem. 286*, 18213−18221.
(40) Otwinowski, Z., and Minor, W. (1997) Processing of X-ray diffraction data collected in oscillation mode. *Methods Enzymol. 276*, 307−326.
(41) Kabsch, W. (2010) XDS. *Acta Crystallogr. D66*, 125−132.
(42) Winn, M. D., Ballard, C. C., Cowtan, K. D., Dodson, E. J., Emsley, P., Evans, P. R., Keegan, R. M., Krissinel, E. B., Leslie, A. G. W., McCoy, A., McNicholas, S. J., Murshudov, G. N., Pannu, N. S., Potterton, E. A., Powell, H. R., Read, R. J., Vagin, A., and Wilson, K. S. (2011) Overview of the CCP4 suite and current developments. *Acta Crystallogr. D67*, 235−242.
(43) Vagin, A., and Teplyakov, A. (2010) Molecular replacement with MOLREP. *Acta Crystallogr. D66*, 22−25.
(44) Emsley, P., Lohkamp, B., Scott, W. G., and Cowtan, K. (2010) Features and development of Coot. *Acta Crystallogr. D66*, 486−501.
(45) Murshudov, G. N., Vagin, A. A., and Dodson, E. J. (1997) Refinement of macromolecular structures by the maximum-likelihood method. *Acta Crystallogr. D53*, 240−255.
(46) Murshudov, G. N., Skubak, P., Lebedev, A. A., Pannu, N. S., Steiner, R. A., Nicholls, R. A., Winn, M. D., Long, F., and Vagin, A. A. (2011) REFMAC5 for the refinement of macromolecular crystal structures. *Acta Crystallogr. D67*, 355−367.
(47) Bricogne, G., Blanc, E., Brandl, M., Flensburg, C., Keller, P., Paciorek, W., Roversi, P., Sharff, A., Smart, O. S., Vonrhein, C., and Womack, T. O. (2011) *BUSTER*, version 2.8.0, Global Phasing Ltd., Cambridge, U.K.
(48) Schüttelkopf, A. W., and Van Aalten, D. M. F. (2004) PRODRG: A tool for high-throughput crystallography of protein-ligand complexes. *Acta Crystallogr. D60*, 1355−1363.
(49) Chen, V. B., Arendall, W. B., Headd, J. J., Keedy, D. A., Immormino, R. M., Kapral, G. J., Murray, L. W., Richardson, J. S., and Richardson, D. C. (2010) MolProbity: All-atom structure validation for macromolecular crystallography. *Acta Crystallogr. D66*, 12−21.
(50) *The PyMOL Molecular Graphics System*, version 1.5 (2010) Schrödinger, LLC, New York.
(51) Kabsch, W. (1976) Solution for Best Rotation to Relate 2 Sets of Vectors. *Acta Crystallogr. A32*, 922−923.
(52) Niesen, F. H., Berglund, H., and Vedadi, M. (2007) The use of differential scanning fluorimetry to detect ligand interactions that promote protein stability. *Nat. Protoc. 2*, 2212−2221.
(53) Frisch, M. J., et al. (2009) *Guassian 09*, Gaussian, Wallingford, CT.
(54) Stephens, P. J., Devlin, F. J., Chabalowski, C. F., and Frisch, M. J. (1994) Ab Initio Calculation of Vibrational Absorption and Circular Dichroism Spectra Using Density Functional Force Fields. *J. Phys. Chem. 98*, 11623−11627.
(55) Becke, A. D. (1993) Density-Functional Thermochemistry. 3. The Role of Exact Exchange. *J. Chem. Phys. 98*, 5648−5652.
(56) Ramadhar, T. R., and Batey, R. A. (2011) Accurate prediction of experimental free energy of activation barriers for the aliphatic-Claisen rearrangement through DFT calculations. *Comput. Theor. Chem. 976*, 167−182.
(57) Cances, E., Mennucci, B., and Tomasi, J. (1997) A new integral equation formalism for the polarizable continuum model: Theoretical background and applications to isotropic and anisotropic dielectrics. *J. Chem. Phys. 107*, 3032−3041.
(58) Fernandez, A., Fraser, C., and Scott, L. R. (2012) Purposely engineered drug-target mismatches for entropy-based drug optimization. *Trends Biotechnol. 30*, 1−7.
(59) Frederick, K. K., Marlow, M. S., Valentine, K. G., and Wand, A. J. (2007) Conformational entropy in molecular recognition by proteins. *Nature 448*, 325−329.
(60) Teague, S. J. (2003) Implications of protein flexibility for drug discovery. *Nat. Rev. Drug Discovery 2*, 527−541.
(61) Freire, E. (2008) Do enthalpy and entropy distinguish first in class from best in class? *Drug Discovery Today 13*, 869−874.
(62) Diederichs, K., and Karplus, P. (1997) Improved R-factors for diffraction data analysis in macromolecular crystallography. *Nat. Struct. Biol. 4*, 269−275.